Kurdistan Region Government -Iraq
Ministry of High Education and Scientific Research
University of Salahaddin -Erbil
College of science
Department of physics

Optical coherence tomography (from technology to application in ophthalmology)

This Research is submitted to the college of Since/University of Salahaddin–Erbil, as part of the Requirement for bachelor's degree in the Department of Physics

Prepared by:

Halima Mudhafar Ahmad

Muhammad Sardar Salih

Supervised by:

MSc. Eman Abdulmajed Saied

May 2024 AD **Ramadan 1445** **Jozardan2724K**

Table of contain

Abstract

Optical coherence tomography from technology to application in ophthalmology Eyes like any organ of body can get sick since the eye parts very complicate and small we thought that it could be different illness especially the retina that are too important part of eyes we thought that need to make a project about it and did it that's why we are in a project talk about the eyes structure and diseases until we can talk about eye diseases detection and also about the historical background optical coherence tomography and physics of device and types of OCT and advantage and disadvantage at the end we collected some data of patient and analysis them we think that it could be better we did to research more with other models of devices to know more physically and patient cases and ways to medicate illness.

Chapter one

1.1General Introduction

The eye is the primary organ of vision. Each one of the two eyeballs is located in the orbit, where it takes up about one-fifth of the orbital volume The remaining space is taken up by the extra ocular muscles, fascia, fat, blood vessels, nerves and the lacrimal gland. The eye is embryo logically an extension of the central nervous system. It shares many common anatomical and physiological proper- ties with the brain. Both are protected by bony walls, have firm fibrous coverings and a dual blood supply to the essential nervous layer in the retina. The eye and brain have internal cavities perfused by fluids of like composition and under equivalent pressures. As the retina and optic nerve are outgrowths from the brain, it is not surprising that similar disease processes affect the eye and central nervous system. The physician should constantly remind himself or herself of the many disease conditions that can simultaneously involve the eye and the central nervous system.

The three coats of the eye are as follows:

(a) **Outer fibrous layer**: • cornea • sclera • lamina cribrosa.

(b) **Middle vascular layer** ("uveal tract"):

• Iris

• ciliary body – consisting of the pars plicata and pars plana

• Choroids.

(c) **Inner nervous layer**:

• pigment epithelium of the retina

• Retinal photoreceptors

• Retinal neurons.

1.2 Structures of Eyes:

The structure of eyes are complex. Each eyes constantly adjusts the amount of light it lets in, focuses on objects near and far, and produced continuous image that are instantly transmit to the brain.

1.2.1 Cornea: A transparent tissue devoid of blood vessels but abounding in nerve cells. Diameter of cornea roughly 12mm and 0.6mm thick at its center. The corneal surface provides, in fact, about 73% of the total refractive power of eye. At the edges refractive index is 1.376, where at entering the eye refractive index changes abruptly from 1 to 1.38.

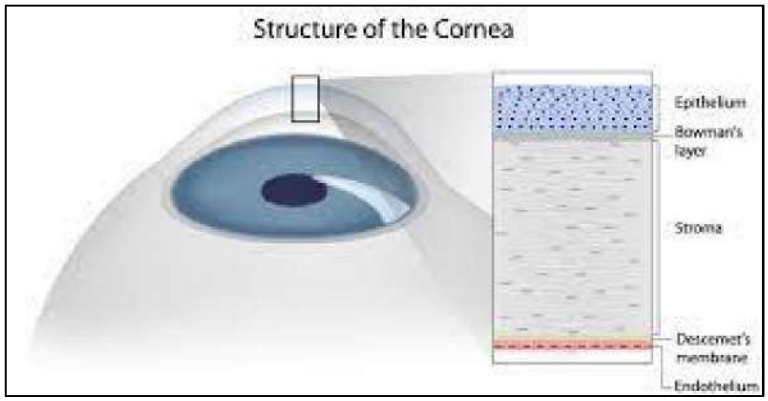

Fig (1.1) structure of cornea.

1.2.2 Iris: is a diaphragm that gives the eye its characteristic color and controls the amount of light that enters. The amount and location of pigment in the iris determine whether the eye looks blue, green, gray or brown.

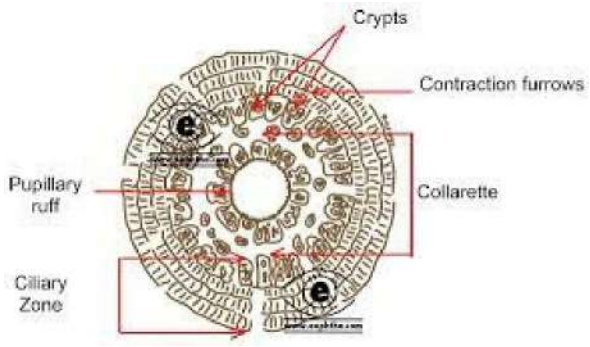

Fig (1.2) structure of Iris.

1.2.3 Pupil: is the black opening in the middle of the iris, and the iris contains two sets of delicate muscles that change the pupil size in response to light stimuli, adjusting the diameter from a minimum of about 2 mm on a bright day to a maximum of about 8 mm under very dark conditions, the adjustable opening in the iris through which the light passes by pupil.

Crystalline lens: is a transparent structure about the size and shape of a small lima bean. The lens provides the fine tuning in the final light focusing process, changing its own shape appropriately to transform an external scene into a sharp image on the retina.

Retina: is that part of the eye and the inner rear layer of the eye, the screen that receives light energy and converts it into electrochemical energy. The retina is a complex nerve-related structure that in essence is an outgrowth of the brain.

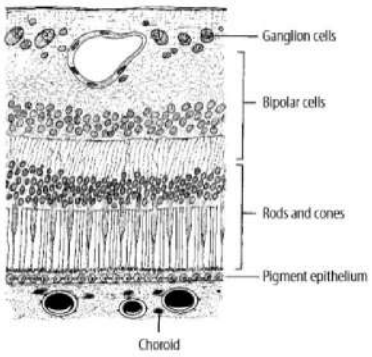

Fig(1.3) retina structure

Sclera: is covered the eye with a tough white coating, that forms the supporting framework of the eye. And protective covering that wraps over most of eyeball.

1.3 Eye Diseases

The diseases or a disorder that destroy eye tissue and other parts of the eyes can be classified as eye diseases. There are different types of eye diseases, which can either be minor, which don't last for a longer time or some can also lead to a permanent loss of vision.

There are different factors behind the causes of eye diseases. These factors include age, stress, infections, heredity, nutritional deficiencies, injuries or accidents, etc.

1.3.1 Long sight and short sight

Hypermetropia (long sight) is associated with certain eye conditions, notably narrow-angle glaucoma and childhood amblyopia of disuse. Myopia (short sight) is associated with other conditions, particularly retinal detachment, cataract and myopic retinal degeneration.

The term "short sight" is used in these instances unwittingly by the layman to mean two different situations; either it can mean presbyopia (caused by diminished focusing power with ageing, as in the case of the old man) or it can mean myopia (caused by a larger eyeball, as in the case of the young lady).the myopic person has physically larger than normal eyes, with an anteroposterior diameter of more than 24 mm, and, by contrast, the hypermetropic (or long- sighted person) person has smaller than usual eyes, with an anteroposterior diameter of less than 24 mm.

hypermetropia and myopia have nothing to do with presbyopia, which is the failure of the eyes to focus on near objects, appearing in middle age. This is nothing to do with the length of the eyeball but is related to a diminished ability to change the shape of the lens. The hypermetropic requires a convex lens to converge the rays, whereas the myopic person requires a concave lens to make light rays diverge before reaching the eye.

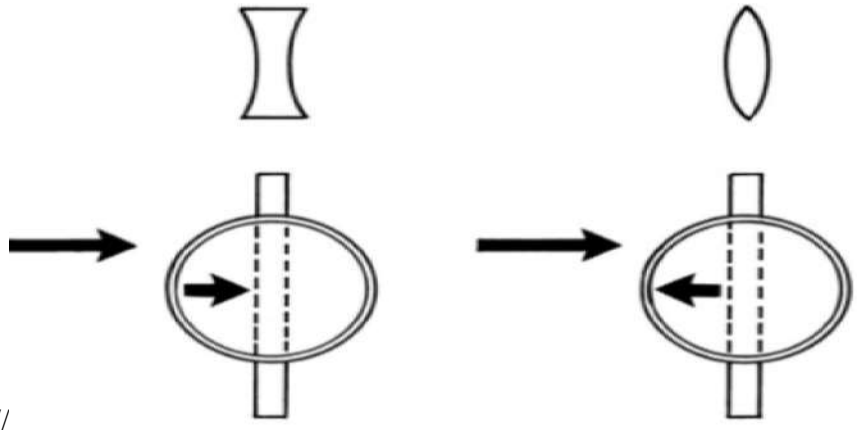

//

Fig.1.4: Concave lens ‘with’; convex lens ‘against’

The Watering Eye

Quite often, patients present at the clinic or surgery complaining of watering eyes. It could be the golfer whose glasses keep misting up on the fairway, the housewife who is embarrassed by tears dropping on food when cooking, or the six-month-old baby whose eyes have watered and discharged since birth. Sometimes an elderly patient might complain of watering eyes when on examination there is no evidence of tear excess but the vision has been made blurred by cataracts. Some degree of tear overflow is, of course, quite normal in windy weather, and the anxious patient can overemphasise this; it is important to assess the actual amount of overflow by asking the patient whether it occurs all the time both in and out of doors. An eye can water because the tears cannot drain away adequately or because there is excessive secretion of tears.

The Dry Eye

A patient might complain of dryness of the eyes simply because the conjunctiva is inflamed, but when the tear film really is defective, the patient might complain of soreness and irritation rather than dryness. The diagnosis of a dry eye depends on a careful examination and it is quite erroneous to assume that the tear film is inadequate simply because the patient complains of dryness, or even if the symptoms appear to be improved by artificial tears. The normal tear film consists of three layers and the integrity of this film is

essential for comfort and more importantly for good vision. The anterior, or outermost, layer is formed by the oily secretion of the meibomian glands and the layer next to the cornea is mucinous to allow proper wetting by the watery component of the tears, which lies sandwiched between the two. This three-layered film is constantly maintained by the act of blinking.

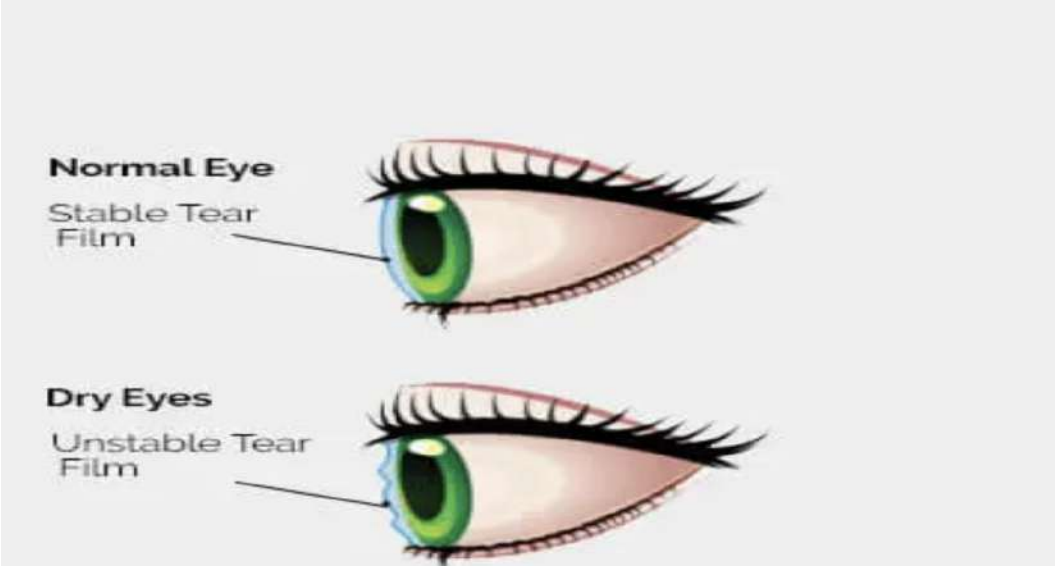

Fig.(1.5) dry eye and normal eye

1.3.2 The Red Eye

Redness of the eye is one of the commonest signs in ophthalmology, being a feature of a wide range of ophthalmological conditions, some of which are severe and sight threatening, whereas others are mild and of little consequence. Occasionally, the red eye can be the first sign of important systemic disease. It is important that every practicing doctor has an understanding of the differential diagnosis of this common sign, and a categorisation of the signs, symptoms and management of the red eye will now be made from the standpoint of the nonspecialist general practitioner.

The simplest way of categoriesing these patients is in terms of their visual acuity. As a general rule, if the sight, as measured on the Snellen test chart, is impaired, then the cause might be more serious. The presence or absence of pain is also of significance, but as this depends in part on the pain threshold

of the patient, it can be a misleading symptom. Disease of the conjunctiva alone is not usually painful, whereas disease of the cornea or iris is generally painful.

The red eye will, therefore, be considered under three headings: the red eye that sees well and is not painful, the red painful eye that can see normally, and the red eye that does not see well and is acutely painful.

1.3.3 OCULAR CHEMICAL BURNS

Chemical burns of the eye are among the few true ocular emergencies. Begin eye irrigation immediately, even before completing the his- tory or measuring the vision. Acid burns cause denaturation of tissue proteins, which act as a barrier to prevent further diffusion. For this reason, they are generally less devastating than alkali burns, but they can still be very severe. Alkali burns do not cause denaturation of tissue proteins. Therefore, caustic alkaline chemicals tend to penetrate deeper than acid bums and tend to be generally more destructive to ocular tissues. They may cause corneal melting, blanching of the conjunctiva, severe corneal scarring, and intraocular complications such as uveitis and secondary glaucoma. Clinical findings in mild burns of either type include conjunctival hyperemia, chemosis and corneal erosions and mild haziness. More severe cases show corneal opacification and limbal ischemia.

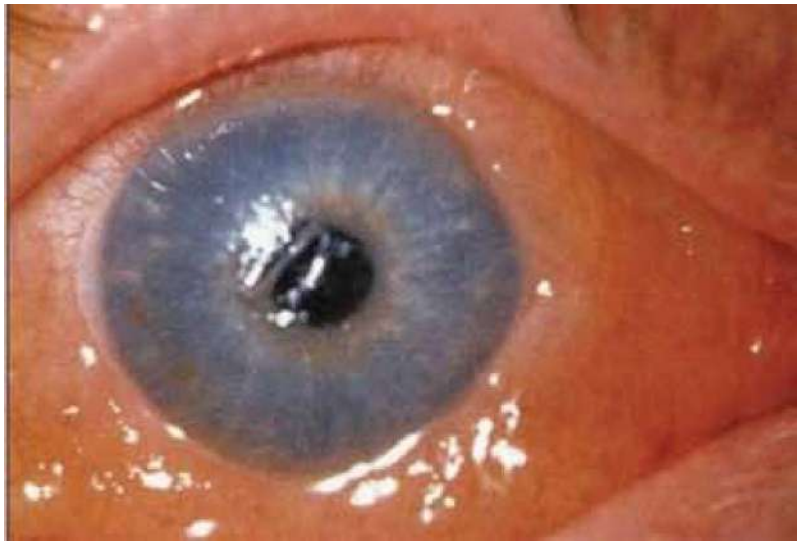

Fig.1.6 ; Alcali burn acute stage chemosis of conjunctiva and mild opacification of cornea.

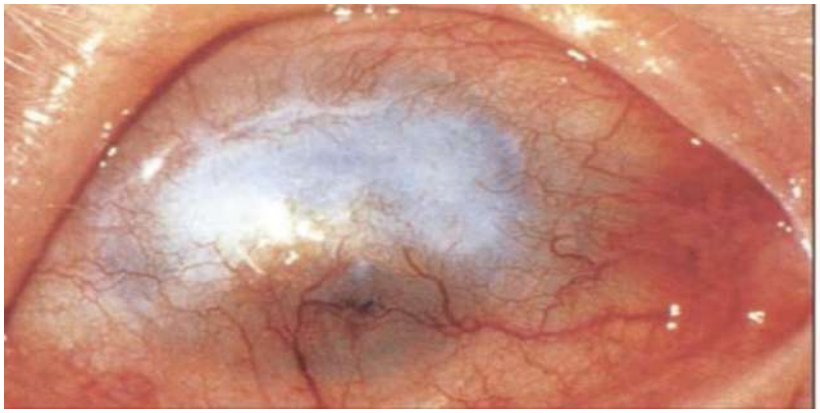

Fig.1.7 ; Alcali burn late stage– total opacification of cornea with neovascularizion on the blind eye.

1.3.4 Glaucoma:

Glaucoma is an eye disease, which causes blindness due to increased intraocular pressure. The color of the optic nerve can be important in determining atrophy of the optic nerve due to glaucoma or other causes. Temporal pallor of the optic nerve, can occur as a result of diseases that damage the nerve fibers, such as brain tumors or optic nerve inflammation, or in conjunction with glaucomatous cupping.

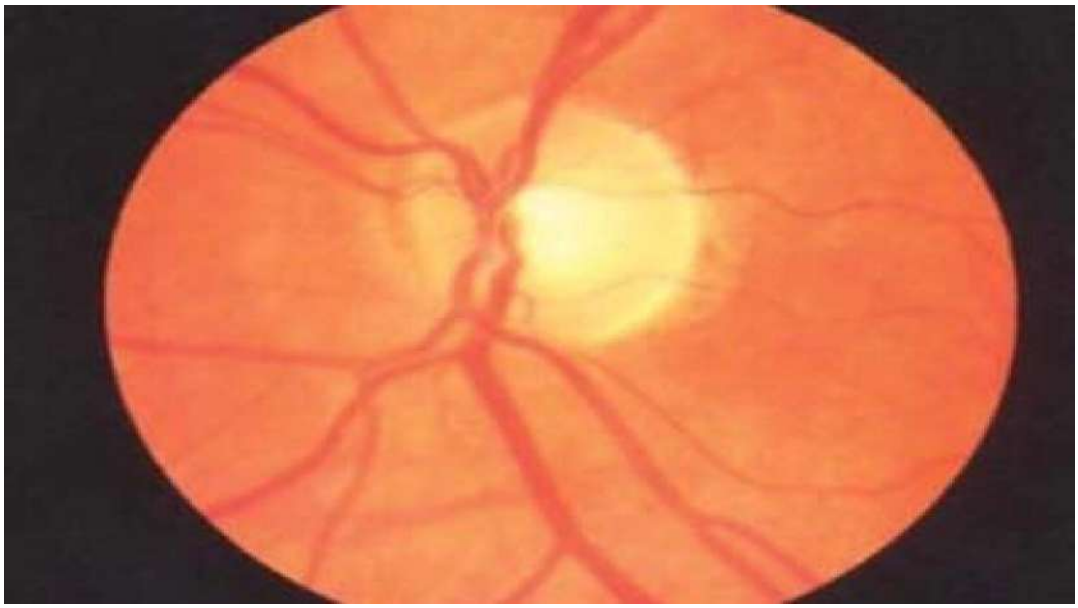

Fig.1.8 ;Temporal pallor of the optic nerve. Diseases that damage optic nerve fibers may result in temporal pallor of the optic nerve. Note the normal nerve color present only on the nasal aspect of the disc.

The term glaucomatous cupping refers to an increase in the size of the optic cup relative to the optic disc that occurs in glaucoma. The increase in the cup is due to loss of nerve fibers bundled in the optic nerve. This so-called cup-disc ratio is determined by comparing the diameter of the disc to that of the cup.

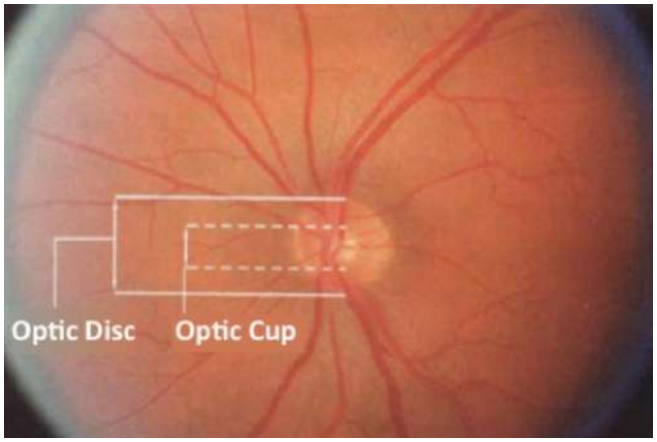

Fig.1.9 Cup-disc ratio. In this non-diseased optic disc, the cup is less than one half the diameter of the disc, indicating absent or low level of suspicion of glaucoma.

The optic discs generally should appear symmetric between the eyes, an asymmetric cup:disc ratios should arouse suspicion of glaucoma. The larger the cup, the greater the probability of a glaucomatous optic nerve. A cup measuring one half the size of the disc or larger (a cup-disc ratio of 0.5 or more)raises suspicion of glaucoma.

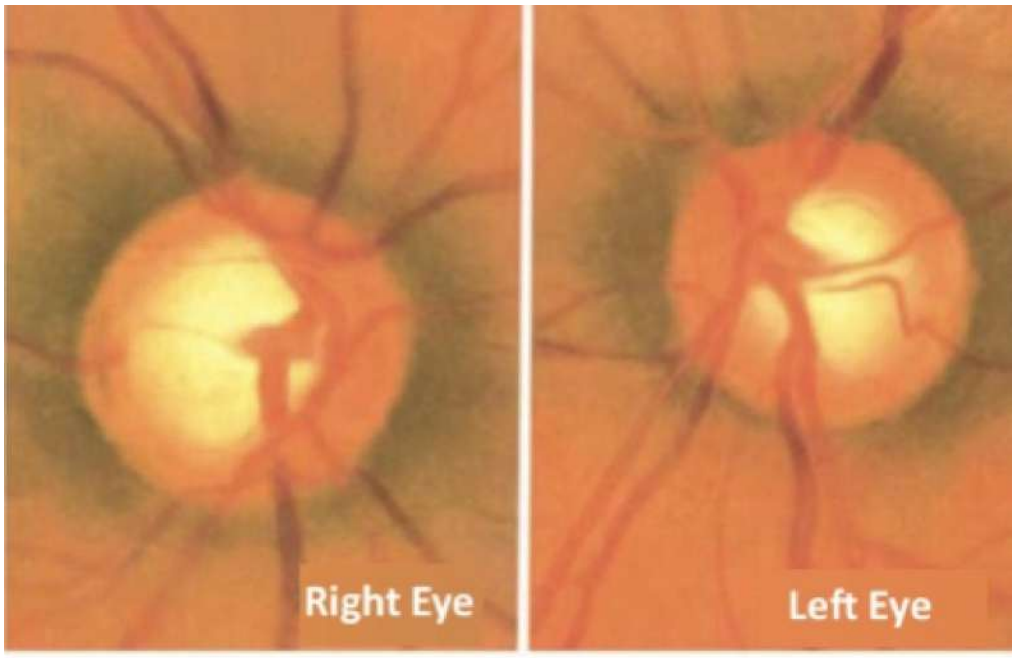

Fig.1.10: Glaucomatous cupping. Patient's right eye shows a cup-disc ratio of 0.8 (high level of glaucoma suspicion); the left eye shows a cup-disc ratio of 0.6 (moderate level of glaucoma suspicion). The asymmetry of cup-disc ratios here also raises suspicion of glaucoma.

Disc hemorrhages are also a possible sign of glaucoma. A large cup should be suspected if central pallor of the disc is prominent. Because the cup is a depressed area of the disc, retinal vessels passing over the disc are seen to bend at the edge of the cup, a useful sign in evaluating cup size.

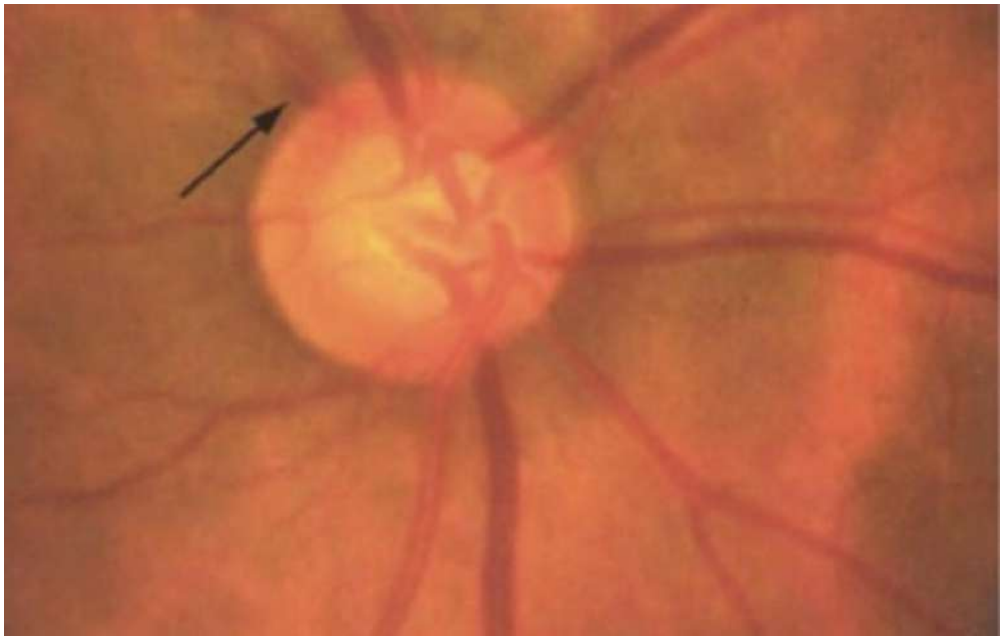

Fig.1.11: Disc hemorrhage. A hemorrhage on the optic disc may indicate glaucomatous damage.

Chapter two (OCT)

Types of OCT

Optical coherence tomography (OCT) imaging is rapid, safe, non-invasive and is increasingly being recognised as the gold standard for diagnosis of retinal disease [Rosenfeld, P.J., 2016]. However, OCT machines have several limitations. First, they are costly; the price of a retinal OCT device ranges from ~£30,000–£100,000 [Olson, J., et.al]. Second, the use of these devices are limited to typical clinical settings such as hospital clinics to optometry practices. They are housed in large tabletop configurations and require alternating current power, constraining their portability. As patients are required to sit upright and stabilise their head on a chinrest whilst maintaining steady fixation, they are only suitable for ambulatory and cooperative patients. Third, a certain level of skill is required to capture optimal images. A technician is often required to align the device, capture the image and perform a quality check to ensure that the image is acceptable. In this review, we discuss several efforts that aim to address these limitations and thus improve the accessibility of this valuable diagnostic tool and enable point-of-care diagnostics, telemedicine and remote monitoring.

❖ Miniature and low-cost OCT

The construction of a portable, handheld, OCT device could increase the ease of access and expand OCT into settings where use is currently prohibited by its cost and size. There are currently three commercial handheld SD-OCT systems available that address this issue. The Envisu C2300 OCT (Leica Microsystems, Germany) became the first handheld OCT scanner to receive clearance from the Food and Drug Administration [Kiernan, D.F.,et.al]. The scanner consists of a 1.5 kg imaging probe connected to a console by a 1.3-m flexible cable with the most recent iteration, the C2300 additionally providing a variety of lenses to enable both anterior- and posterior-segment imaging. The iVue system by Optovue Inc. consists of a stand-mounted unit

with a 2.2-kg removable scanner [Maloney, R., 2012.]. Both systems benefit from rapid acquisition speed facilitating capture in paediatric populations. A third device, the Heidelberg Spectralis Flex Module (Heidelberg Engineering, Heidelberg, Germany) incorporates a flexible 'boom' arm, which houses the acquisition lens and can be adjusted up to 100 cm from the main device body (Fig. 2.1) [Liu, X., et.al.]. The portability of all these devices has allowed for imaging of patients in different positions and beyond the outpatient clinic, from intensive care to the surgical environment [Dayani, P.N., et.al]. However, these handheld systems are associated with a steep learning curve for operation, are subject to motion artifacts and are still considerably heavy to hold or are attached to much larger systems that restrict use outside of the clinic.

Fig.2.1 Heidelberg Engineering Spectralis Flex Module in use. The system is affixed to a moveable stand with a flexible arm. Images courtesy of Dr Xiaoxuan Liu and Dr Aditya Kale, University Hospitals Birmingham NHS Foundation Trust.

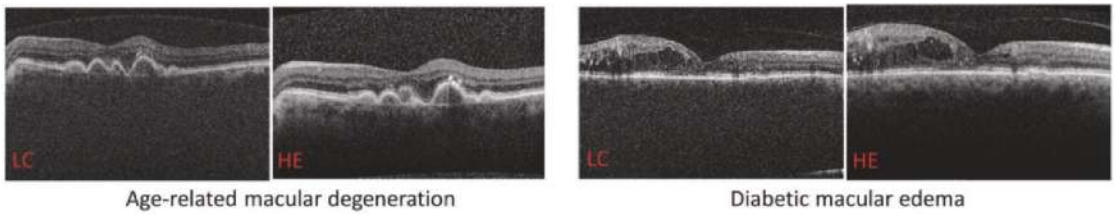

Fig. 2.2 Representative images from patients with pathology that were acquired by the low-cost OCT (LC) and the Heidelberg Engineering Spectralis (HE) systems. Scale bars: 500 μm. Images courtesy of Prof. Adam Wax, Duke University.

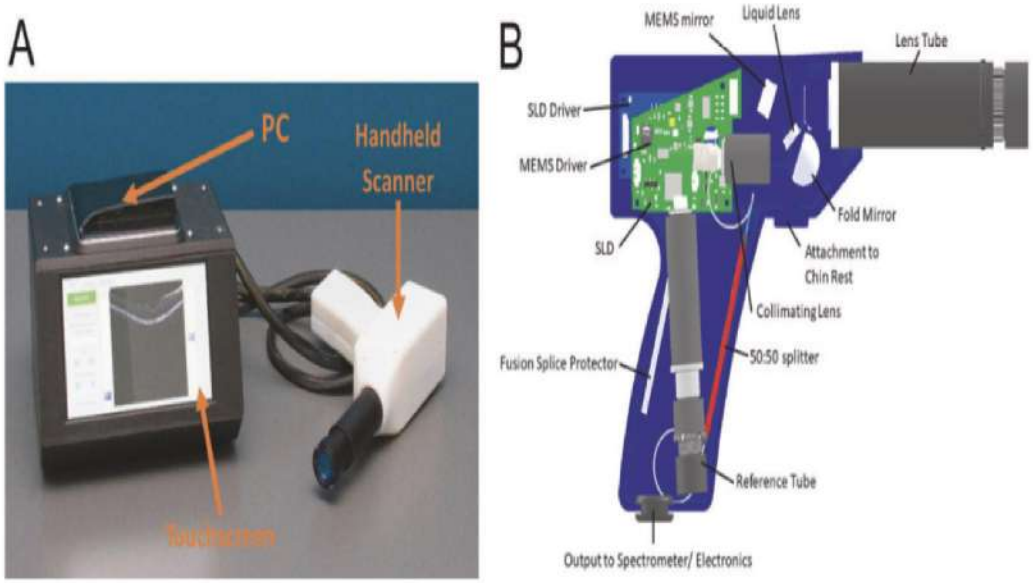

Fig. 2.3 Low-cost, handhled OCT system developed by Duke University. A Complete low-cost OCT system showing PC, touchscreen and scanner. B Detailed composition inside the low-cost OCT handheld scanner. Images courtesy of Prof. Adam Wax, Duke University.

❖ Automated OCT

Much of the burden of chronic eye conditions to both patients and to healthcare systems may be attributed to the limitations of the current eye examination. Patients with such conditions commonly require long term monitoring with frequent, time-consuming visits to the eye clinic. The

workflow in many eye clinics is inefficient, with patients being asked to wait multiple times, interact with several different healthcare staff and see their doctor on multiple occasions. The need for extensive testing also results in large staffing and equipment costs and extensive floor space requirements. Moreover, the fundamental unit of the eye examination slit-lamp ophthalmoscopy has little changed since its original description in 1911 by Gullstrand [Timoney, P.J,et.al], being time-consuming, subjective, non-quantitative and requiring an experienced clinician. A new form of eye examination has been developed by Envision Diagnostics, Inc. (El Segundo, CA, USA) termed binocular OCT [Walsh, A.C., 2011.], that aims to address the shortcomings of the current eye exam, and adds many unique capabilities.

A prototype of this system has undergone usability testing among patients with chronic eye conditions and healthy volunteers [Chopra, R. , et.al]. Unlike other OCT devices, the binocular OCT prototype consists of two oculars that align to the patient's eyes in an automated manner, enabling a pair of eyes to be imaged simultaneously. This reduces the labour required to align the device, and also reduces the overall scan time. The binocular OCT also utilises a tuneable swept-source laser system with adjustable optics that can switch from anterior eye imaging to lens imaging, to vitreous imaging and to posterior pole imaging, permitting whole-eye OCT without the need for additional attachments. Furthermore, the device incorporates 'smart technology', offering more advanced display, input and computing capabilities than conventional OCT. A speaker system is used to deliver audio instructions to guide the automated examination. In addition, the binocular aspect of the device can be exploited so that OCT imaging can be used for novel applications such as diagnostic functional tests including pupillometry [Chopra, R., et.al] (Fig. 2.4), strabismus measurement and ocular motility [Chopra, R., et.al]. Traditionally these tests have been subjective and required significant clinical expertise to interpret.

With these features, the binocular OCT aims to incorporate many aspects of the eye examination into a single automated, patient-facing instrument, and has a number of potential benefits if this was adopted in tertiary eye-care clinics, including:

● Increased efficiency of eye clinics, allowing patients with chronic eye disease to spend less time waiting during routine hospital eye examinations.

● Reduced costs, through a reduction in the total number of diagnostic instruments required and their associated labour costs.

● Improved quality of eye care, through the introduction of more, quantitative, standardised ocular measurements and high-resolution imaging.

The results of a usability study, and related focus group testing, make it clear that patients are receptive to the concept of an automated eye examination. To be attractive to users, easy to use and effective at performing automated eye examinations, the system will need to be quick, responsive and comfortable. Once established, binocular OCT will offer objective, quantifiable information about almost every aspect of the eye examination and has the potential to supersede many traditional but flawed testing methods. It is unlikely that the automated eye examination will be suitable for use in all patients. However, if such a system can replace some aspects of the eye examination, workflows and waiting times are likely to improve and costs are likely to reduce.

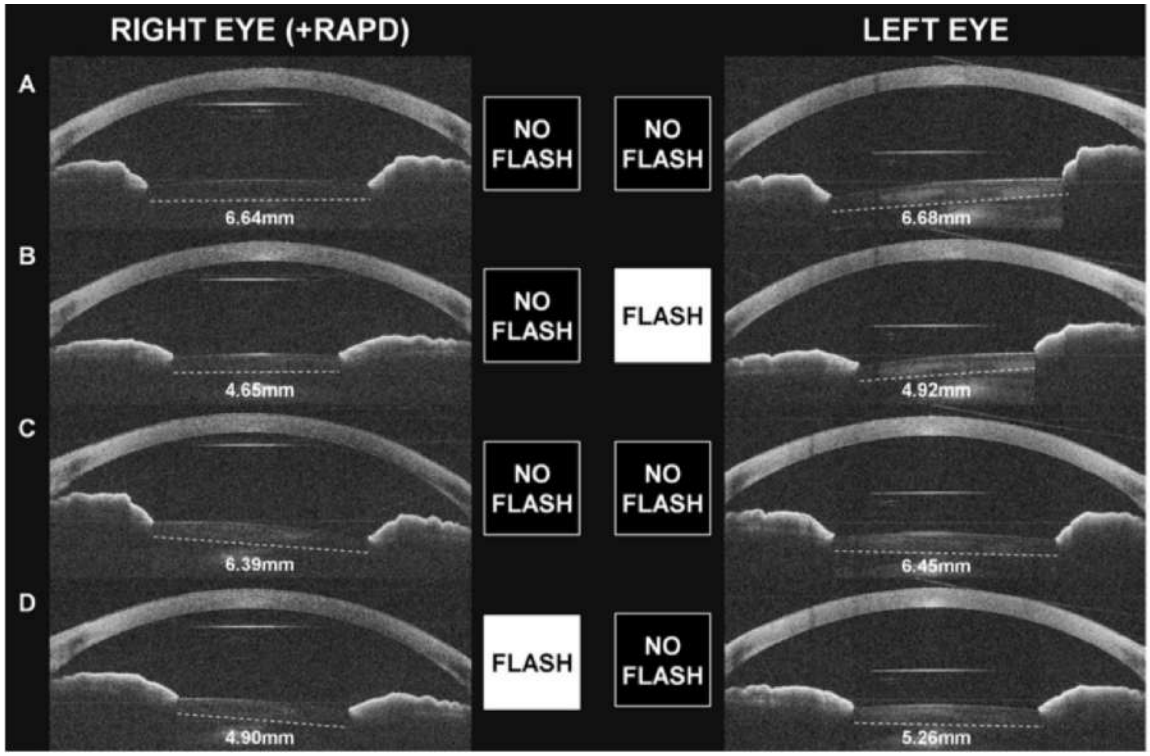

Fig. 2.4 Pupillometry in a patient with a right relative afferent pupillary defect (RAPD), using the binocular optical coherence tomography system. A Resting diameters pre-stimulus; B flash pre- sented to the left eye, constriction of both pupils observed; C both pupils dilated to their resting diameter; D flash presented to the right eye. Constriction amplitude of both eyes is less than that observed when the flash was presented to the left eye.

❖ Home OCT

At-home disease monitoring devices are also in development and may be more cost-effective for monitoring patients at high-risk of developing neovascular AMD [Wittenborn, J.S., et.al]. Notal Vision (Tel Aviv, Israel) received FDA approval for the Fore See Home in 2010, an at-home digital macular visual field and hyperacuity testing device that transmits data directly to the ophthalmologist. The device has since undergone a randomised clinical trial, concluding that individuals at high risk of conversion to neovascular AMD would benefit from a home monitoring strategy for earlier detection of choroidal neovascularisation development . Notal also plans to launch a 'Home OCT' device, a self- operated SD-OCT device that could be provided to patients at risk of vision loss from AMD, or between visits to the ophthalmologist to customise appointments to the individual patient's needs (Fig. 5) [Chopra, R., et.al]. The device acquires images of the central 10 degrees of the macula and subsequently reads the image using the company's artificial intelligence platform, Notal OCT Analyzer (NOA). In a prospective clinical trial, 90% of 196 patients were able to obtain a gradable image in at least one eye after a 2-min video tutorial [Chopra, R., et.al]. When evaluated on images of AMD taken using the device, NOA demonstrated >97% sensitivity and specificity for detection of intraretinal and sub- retinal fluid [Lally, D., et.al]. The device received Breakthrough Device Designation by the FDA in 2018, expediting assessment and review for 510(k) clearance and market authorisation. Though, the usability and validation of the OCT device and software is yet to be determined through peer-reviewed publications. Self-examination low-cost full-field OCT (SELF-OCT) is another proposed low-cost system that allows the patient to independently examine the disease progression of AMD at home without the presence of a physician [Sudkamp, H., et.al]. In contrast to commercially available systems, the SELF-OCT

system sequentially acquires transversal en face images at different depths instead of cross-sectional images in the axial direction. The SELF-OCT prototype device captures images at an axial resolution of 9.1 μm and a transversal resolution of 6.4 and 12.8μm, respectively; although, in vivo retinal scans from the system exhibit more artifacts and a greater signal-to-noise ratio than clinical OCT systems. Furthermore, the field of view of the SELF-OCT is 1.4 × 4.8 × 1.5 mm, which is considerably smaller than clinical OCT systems, but may be sufficient for monitoring of wet AMD . This technology has been patented and is being commercialised by Visotec [von der Burchard, C.C., et.al].

A proposed novel home-based SD-OCT system termed ‘sparse OCT’ has recently been developed by a Swiss group (Fig. 2.6) [Maloca, P., et.al]. The portable device, named MIMO-OCT, generates single 5-mm line scans at a resolution of 400 pixels, or small sample 3.8 × 3.8-mm volume scans at a resolution of up to 150 × 150 pixels. The downsampled scanning pattern is less dense than scan protocols available on commercial SD-OCT systems, but reduces the size of the instrument and enables fast scanning. The prototype required the subject’s head to be inclined downwards onto the headrest, enabling stable positioning to reduce moving artifacts. Manually graded central retinal thicknesses from sparse OCT data in 30 AMD patients were compared to automated measurements obtained from the Heidelberg Spectralis device, showing no statistical difference. Sparse OCT may be one method of delivering a portable at-home OCT system with adequate resolution for monitoring.

Fig. 2.5 Proposed Home OCT, Notal Visio

Fig. 2.6 Home-based MIMO-OCT system. Images courtesy of Dr Peter Maloca, University of Basel.

Physics of OCT:

Principles of Operation and Technology of Optical Coherence Tomography

Because the velocity of light is extremely high, its echo time delay cannot be measured directly by electronics as in ultrasound. The velocity of sound in water is approximately 1500 m/sec, whereas the velocity of light is approximately 3*108 m / sec. Distance or spatial information may be determined from the time delay of reflected echoes according to the formula $\Delta T=z/v$ where ΔT is the echo delay, z is the distance that the echo travels, and v is the velocity of the sound wave or light wave. The measurement of distances or dimensions with a resolution on the 100 - micron scale, which would be typical for ultrasound, corresponds to a time resolution of approximately 100 n sec (100*10^-9 sec) . The echo time delays associated with light are extremely rapid. For example, the measurement of a structure with a resolution on the 10-micron scale, which is typical in OCT, corresponds to a time resolution of approximately 30 f sec (30*10^-15 sec). Direct electronic detection is not possible on this time scale. Instead, it is necessary to use correlation or interferometry techniques. One method for measuring the echo time delay of light is to use low-coherence interferometry. Low - coherence interferometry was first developed for measuring reflections in fiber optics and optoelectronic devices [YOUNGQUIST, R.C., et.al- Gilgen, H.H., et.al]. The first applications of low – coherence interferometry in biomedicine were in ophthalmology to perform precision measurements of axial eye length and corneal thickness [Fercher, A.F., et.al, Huang, D., et.al].

Low-coherence interferometry measures the echo time delay and intensity of backscattered light by comparing it to light that has traveled a known reference path length and time delay. Measurements are performed using a Michelson type interferometer (Figure 2.7) . Light from a source is directed onto a beam splitter and one of the beams is incident onto the sample to be imaged, while the second beam travels a reference path with a variable path length and time delay. The backscattered light from the sample is interfered with reflected light from the reference arm and detected with a photodetector at the output of the interferometer. If the light source is coherent, then interference fringes will be observed as the relative path lengths are varied. However, if low - coherence or short pulse light is used, then interference of

the light reflected from the sample and reference path can occur only when the two path lengths match to within the coherence length of the light. The echo time delay and intensity of backscattered light from sites within the sample can be measured by detecting and demodulating the interference output of the interferometer while scanning the reference path length.

Figure P shows a schematic illustrating how OCT performs cross - sectional imaging. The optical beam is focused into the sample being imaged, and the echo time delay and intensity of the backscattered light are measured to yield an axial backscattering profile. The incident beam is then scanned in the transverse direction, and the axial backscattering profile is measured at several transverse positions to yield a two-dimensional data set. This data set

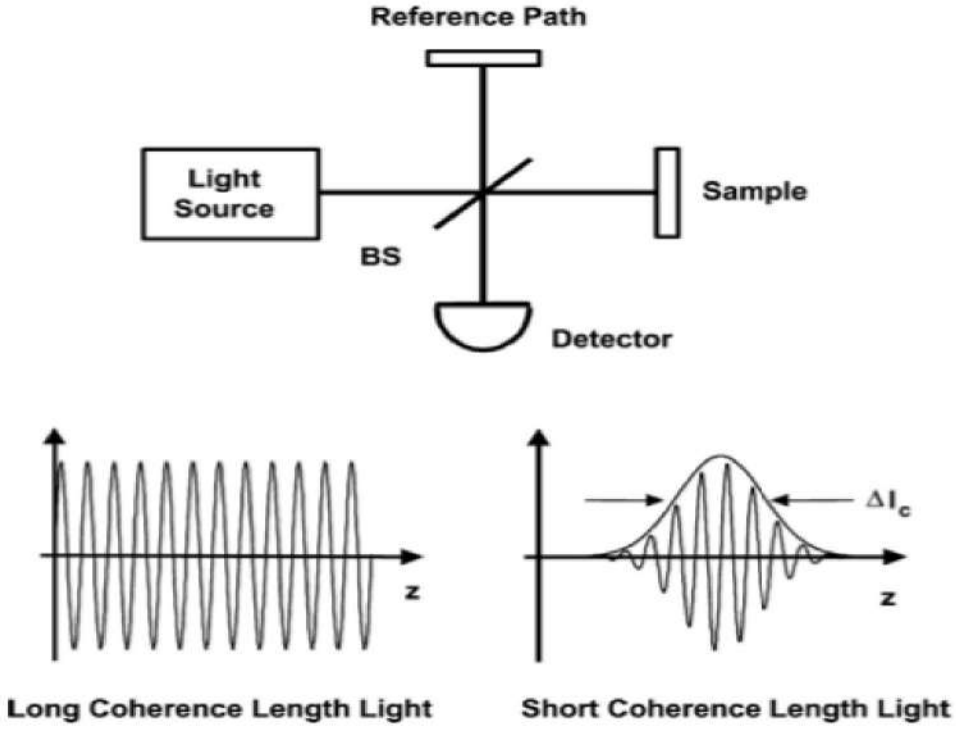

Figure 2.7. OCT performs imaging by measuring the echo time delay of reflected light using low - coherence interferometry. The system is based on a Michelson type interferometer. Reflections or backscattering from the object being imaged are correlated with light which travels a reference path.

represents the optical backscattering through a cross section of the tissue. The data is displayed as a logarithmic gray scale or false color image.

In contrast to conventional microscopy, the mechanisms which govern the axial and transverse image resolution in OCT are decoupled. The axial resolution in OCT imaging is determined by the coherence length of the light source so high resolution can be achieved independent of the beam focusing conditions. The interference signal detected at the output of the interferometer is the electric-field autocorrela- tion of the light source. The coherence length is the spatial width of this field autocorrelation. In addition, the envelope of the field autocorrelation is equivalent to the Fourier transform of the power spectrum. Thus, the width of the autocorrelation function, or the axial resolution, is inversely proportional to the width of the power spectrum. For a source with a Gaussian spectral distribution, the axial resolution Δz is:

Δz =(2ln2/π)(ƛ^/Δƛ)

where Δz and Δƛ are the full widths at half maximum of the autocorrelation function and power spectrum respectively and ! is the source center wavelength. The axial resolution is inversely proportional to the bandwidth of the light source, and thus high resolution may be achieved by using broad bandwidth optical sources.

The transverse resolution achieved with an OCT imaging system is determined by the focused spot size as in conventional microscopy. The transverse resolution is:

Δx=(4ƛ/π)(f/d)

where d is the spot size on the objective lens and f is its focal length. High transverse resolution can be obtained by using a large numerical aperture and focusing the beam to a small spot size. In addition, the transverse resolution is also related to the depth of focus or the confocal parameter b:

b=πΔx^2/2ƛ

Increasing the transverse resolution (smaller Δ x) produces a decrease in the depth of focus, as in conventional microscopy.

Finally, the signal - to - noise of detection can be calculated using standard techniques from optical communications theory and is given by:

SNR =10log(Ɒp/2HυNEB)

where P is the detected power, NEB is the noise equivalent bandwidth of the detection, ŋ is the detector quantum efficiency, and h# is the photon energy. The signal - to - noise ratio scales with the reflected or backscattered power divided by the noise equivalent bandwidth of the detection. This means that higher image acquisition speeds or higher image resolutions require higher optical powers for a given signal- to-noise ratio.

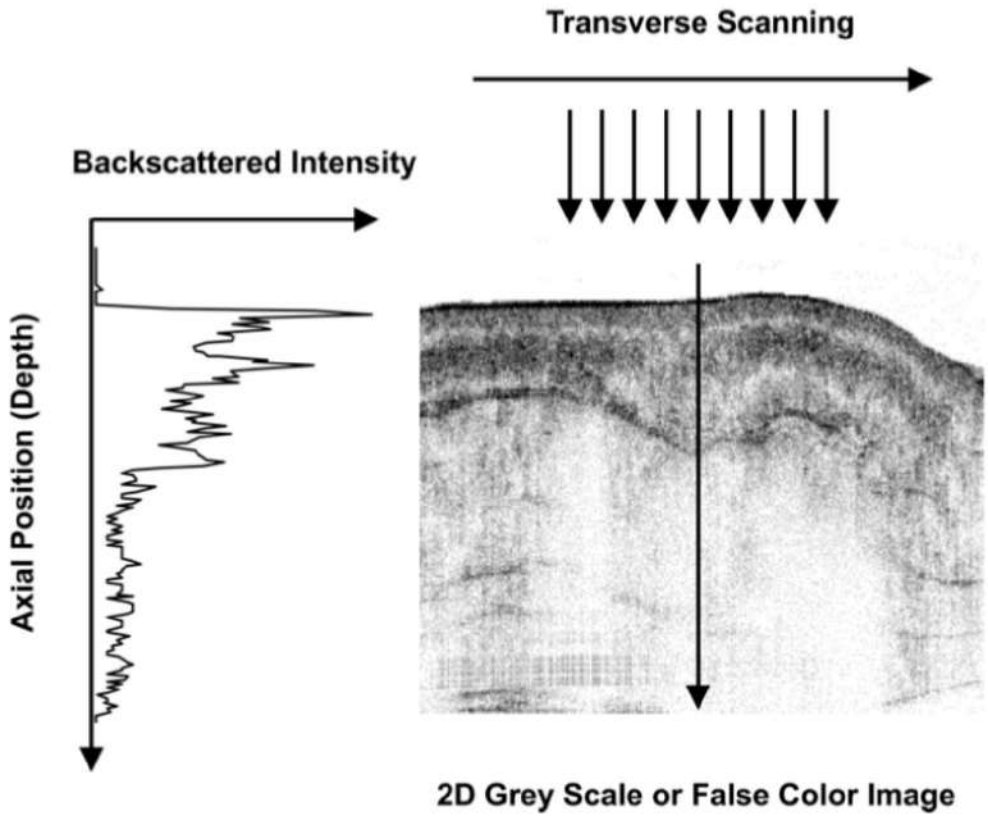

Figure 2.8 Cross - sectional images are constructed by performing measurements of the echo time delay of light at different transverse positions. The result is a two - dimensional data set which represents the backscattering in a cross - sectional plane of the tissue. This data can be displayed as a gray scale or false color image.

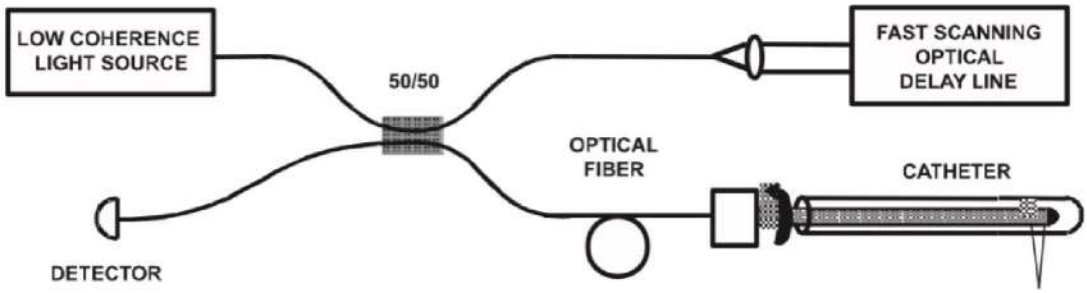

Figure 2.9 Schematic of OCT instrument based on a fiber optic implementation of a Michaelson interferometer. One arm of the interferometer is interfaced to the measurement instrument and the other arm has a scanning delay line. The system shown is configured for high - speed catheter / endoscope - based imaging. The technology can be engineered into a compact and clinically viable form.

Advantage of OCT:

One of the advantages of OCT is that it can be implemented using compact fiber optic components and integrated with a wide range of medical instruments. Figure Q shows a schematic of an OCT system using a fiber optic Michelson type interferometer. A low - coherence light source is coupled into the interferometer and the interference at the output is detected with a photodiode. One arm of the interferometer emits a beam which is directed and scanned on the sample which is being imaged, whereas the other arm of the interferometer is a reference arm with a scanning delay line.

For research applications, short pulse lasers are used as light sources for OCT imaging because they have extremely short coherence lengths and high output powers, enabling high - resolution, high - speed imaging. Many of our studies were performed using a short pulse Cr4 + : Forsterite laser. This laser produces output powers of 100 mW generating ultrashort pulses at wavelengths near 1300 nm and can produce bandwidths sufficient to achieve an axial resolution of 5 to 10 "m [Bouma, B.E., et.al]. Using incident powers in the 1 to 10 mW range, image acquisition speeds of several frames per second and signal - to - noise ratios of 100 dB are achieved. In other studies, a short pulse Ti: Al2O3 laser operating near 800 nm has been used to achieve axial resolutions as fine as 1 "m [Drexler, W., et.al] . For clinical applications, compact superlumines-cent diodes or semiconductor - based light sources are more convenient than short pulse lasers. Commercially available (AFC Technologies, Hull, Quebec, Canada) sources operating at 1300 nm can achieve axial resolutions of ~15 "m with output powers of 10 to 15 mW, sufficient for real - time OCT imaging.

Disadvantage of OCT

While optical coherence tomography (OCT) is a valuable imaging technique, it does have some limitations. These include limited penetration depth in certain tissues, the potential for image artifacts, and the need for skilled interpretation by trained professionals. Additionally, the equipment can be expensive, and the imaging process may require patient cooperation due to the need for precise positioning.

Chapter Three

OCT data analysis

1. OCT Angiograms

a. Vitreoretinal interface: -

This representation permits analysis of the vitroretinal interface. In normal findings no vascular structures are displayed there. In OCT angiography, verifiable vascular networks always indicate a pathological change on the vitroretinal interface.

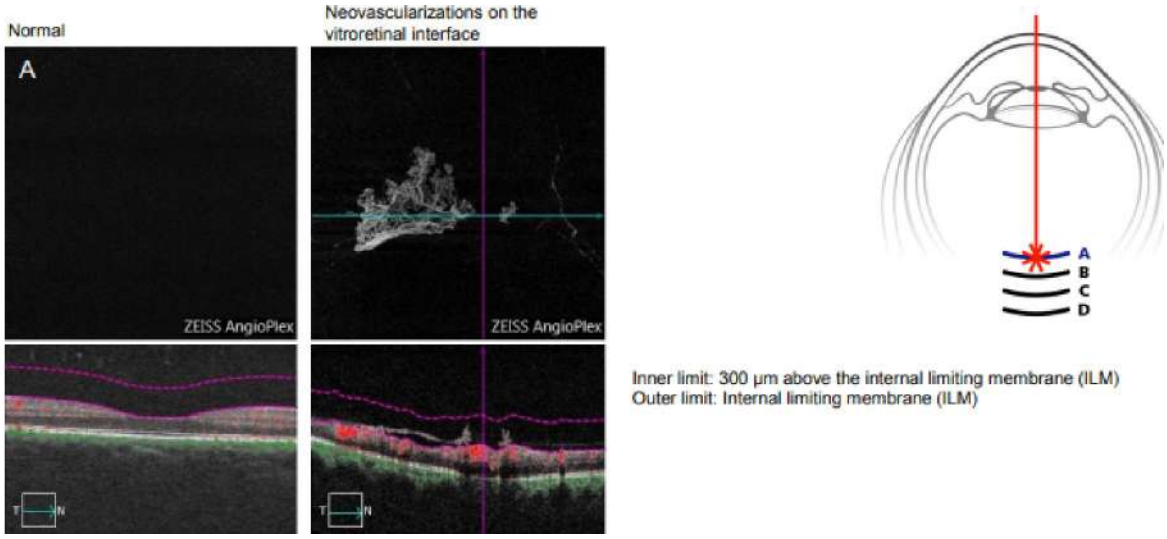

Fig. (3.1) Vitreoretinal interface

B. Neurosensory retina

This representation examines the neurosensory retina. This provides an initial complete overview of pathological changes within the retina, e.g. - Damage to vascular networks (e.g. ischemic areas, see arrow) - Ingrowths of pathologically changed vessels from the choroid.

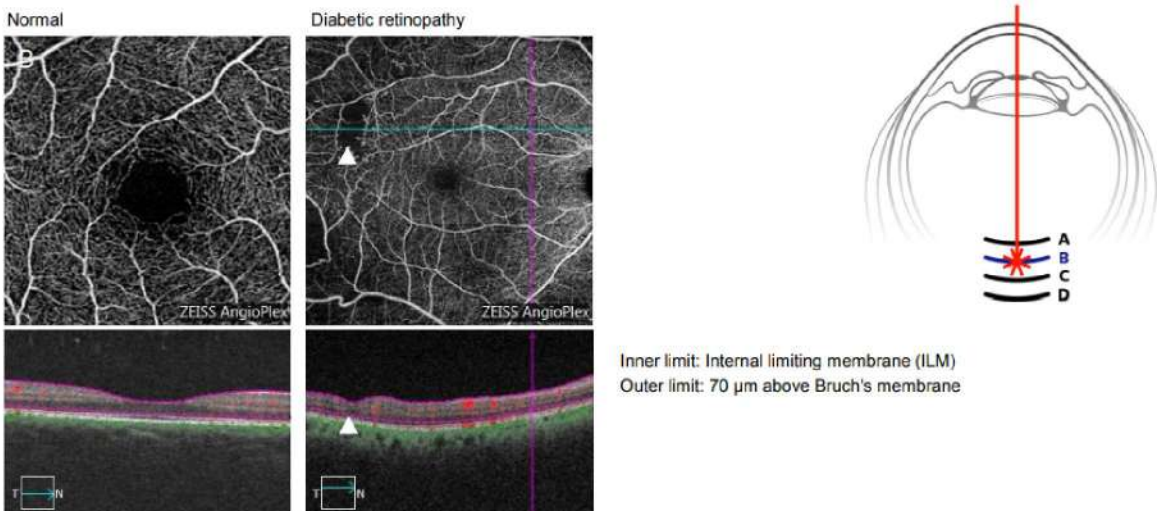

Fig. (3.2) Neurosensory retina

C. Chorio capillaris.

The choriocapillaris is a thin vascular layer which is only several micrometers thick and, in normal findings, exhibits a regular, homogeneous and netlike vascular pattern. In the case of pathological changes such as the occurrence of neovascular structures, significant deviations from this homogeneous pattern occur

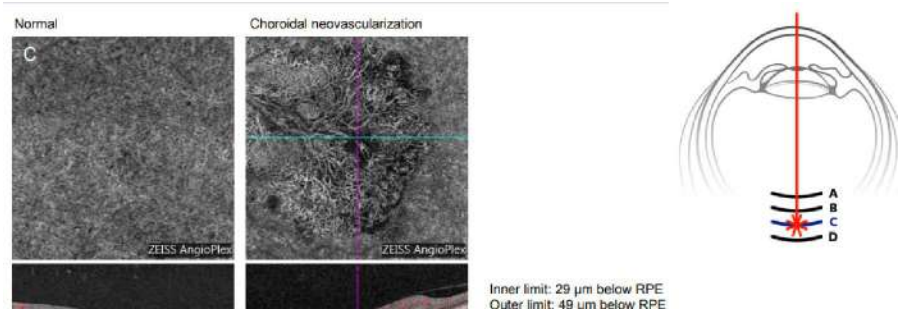

Fig. (3.3) Choriocapillaris

Choroidal neovascularization (CNV) is part of the spectrum of exudative age-related macular degeneration (AMD) that consists of an abnormal growth of vessels from the choroidal vasculature to the neurosensory retina through the Bruch's membrane.

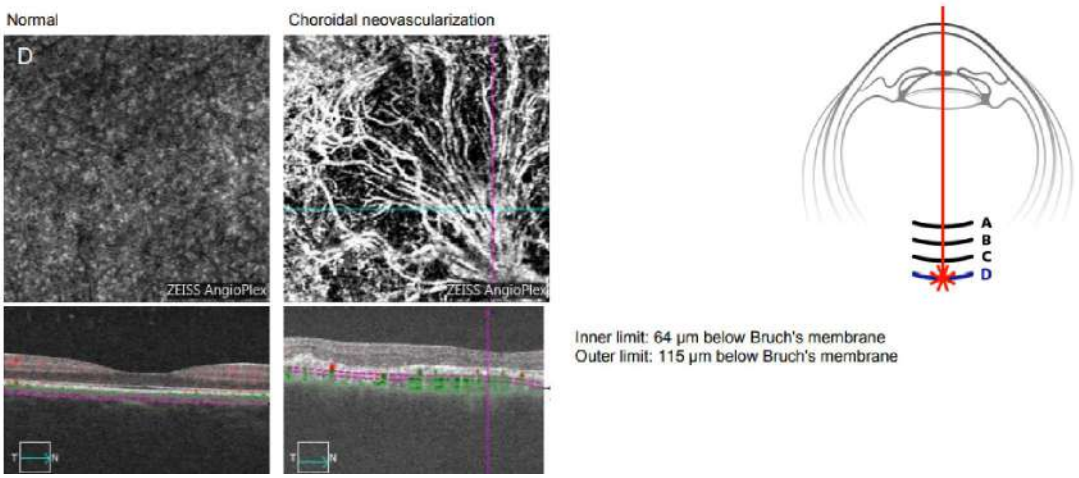

Fig. (3.4) Choroidal neovascularization (CNV)

Color code

It has been compared to *in vivo* optical biopsy. As the resolution of OCT has been getting more and more refined; the identification,

detection, localization and quantification of the tissues has accordingly, become more superior and reliable. The OCT scan printout bears a pseudo-color imaging and retinal mapping is based on different color codes (white, red, orange, yellow, green, blue, and black in order); white being the thickest (>470 microns) and black being the thinnest (<150 microns). The color code distribution is given in Fig. 3.5.

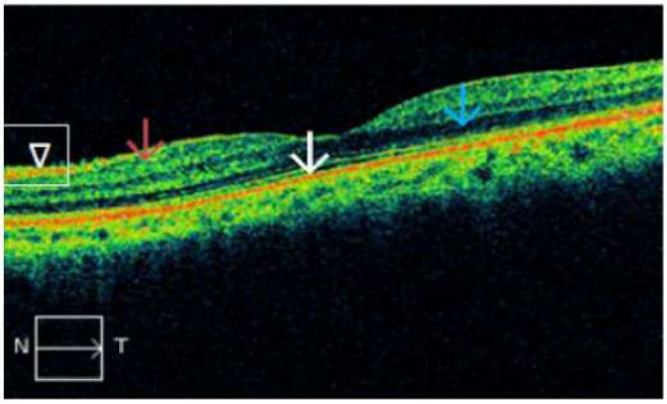

Figure 3.5: Color codes: Red - High reflectivity (white arrow); black– low reflectivity (blue arrow); green - intermediate reflectivity (magenta arrow). Normal retinal structures are labeled as: red for RNFL (arrowhead) and junction of inner and outer segments of photoreceptors (PR); green for plexiform layers (magenta arrow), and blue/black for nuclear layers (blue arrow). N: Nasal. T: Temporal

Normal retinal structures are labeled as: red for RNFL, and junction of inner and outer segments of photoreceptors (PR); green for plexiform layers, and blue/black for nuclear layers. Both PR junctions and retinal pigment epithelium (RPE) are represented by red lines, the former is thinner and the latter is thicker. It is not possible to identify the laterality of the eye from the macular scans. This should always be checked with fundus video image of the scan. Light rays from OCT can reasonably penetrate mild ocular media opacities like cataract, posterior capsular opacification, vitreous hemorrhage, asteroid hyalosis and vitritis.

Indications

Optical coherence tomography provides both qualitative (morphology and reflectivity) and quantitative (thickness, mapping and volume)

analyses of the examined tissues in-situ and in real time. The indications of OCT include posterior segment lesions like the detection of fluid within the retinal layers or under the retina (which may not be visible clinically),3 macular holes, pseudoholes, epiretinal membranes (ERMs), vitreo-macular adhesion (VMA), vitreo- macular traction (VMT), retinoschisis, retinal detachment, diabetic retinopathy (DR), age-related macular degeneration (ARMD), retinal nerve fiber layer thickness (RNFLT), optic disc parameters, as well as assessment and analysis of anterior segment structures like anterior chamber area, volume and iris thickness. OCT cannot be and should not be interpreted independently in reference to any ocular disease. Also, it should never be taken as the only criteria for the diagnosis or treatment of any ocular pathology. The clinician must have other information available such as valid perspectives of patients' systemic and ocular disease, fluorescein angiography (FA), indocyanine green angiography (ICGA), biomicroscopy; and above all, the relevant history of the disease process.

a. Reflectivity The normal ocular tissues which show high reflectivity are: a) the retinal nerve fiber layer; b) the internal limiting membrane; c) the junction between the inner and outer segments of PRs, probably due to densely stacked disc membranes in the outer segments;4 and d) retinal pigment epithelium-Bruch's membrane-choriocapillaries complex. High reflectivity is also a feature of reduced retinal thickness (as in retinal atrophy) and scar tissue. Lesions showing high reflectivity may be superficial, intraretinal or deep retinal. The superficial lesions include; epiretinal and vitreal membranes, exudates and hemorrhages (Fig. 3.6), and cotton wool spots (Fig. 3.6), which are exudates at the margin of ischemic areas. While the intraretinal lesions include; hemorrhages, hard exudates (these are lipoproteins located at the margin between healthy and edematous retina), and retinal fibrosis and disciform degenerative scars. On the other hand, the deep lesions include; a) Drusen, b) retinal pigment epithelial hyperplasia, c) intraretinal and subretinal neovascular membranes, d) scarring following choroiditis, e) trauma or laser treatment, and f)

hyperpigmented choroidal nevi. The lesions causing hypo or low reflectivity include: a) atrophic RPE (loss of pigment); b) cystic or pseudocystic areas containing serous fluid

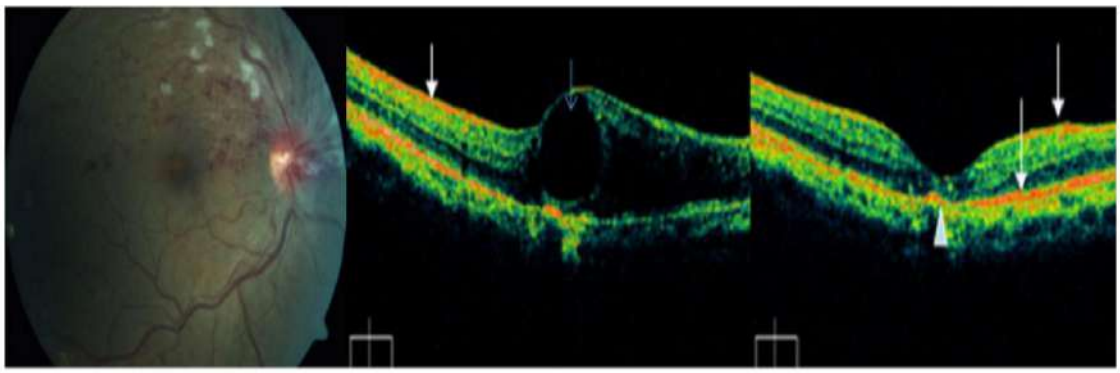

Figure 3.6: Superior hemi-central retinal venous occlusion. Fundus photo shows classical superficial and deep retinal hemorrhages with cotton wool exudates. Middle: OCT image shows a large cystic swelling of the retina (blue arrow). White arrow indicates signal from retinal hemorrhage. Right: OCT image of the same eye after intravitreal injections of bevacizumab, showing markedly resolved edema with residual subfoveal scarring (white arrow head).

The application of OCT has gone beyond the borders of ophthalmology. Ocular manifestations of systemic diseases are widely accepted as important clues to the diagnosis, treatment and follow up of such disorders. OCT has added a new dimension in this field. Few examples from hematological (Fig. 3.7) and neurological disorders (Fig. 3.8) have been cited in this article, but the list is much more extensive**.**

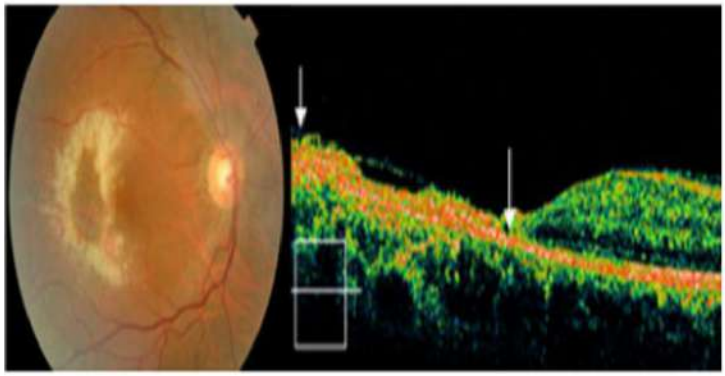

Figure 3.7: OCT in systemic disease (acute lymphoid leukemia): Fundus photo: ring shaped retinal opacification, with hemorrhages, attributed to leukemic cell infiltration and possible CMV retinitis. OCT shows marked retinal atrophy and a hyperreflective scar (between arrows).

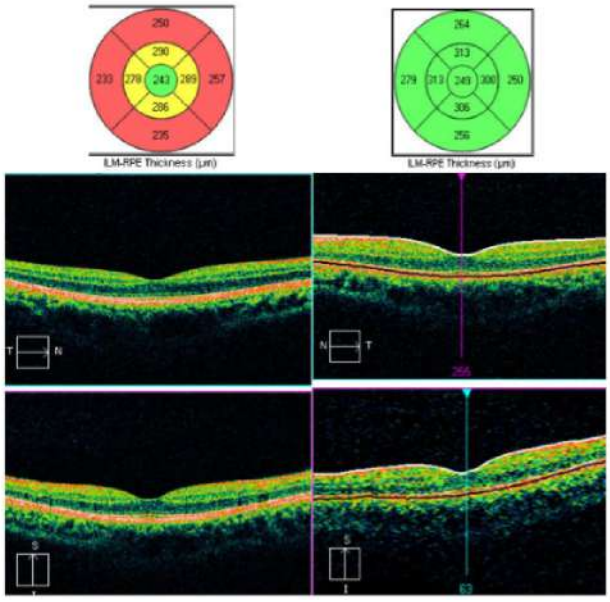

Figure 3.8: OCT image in a patient with multiple sclerosis. Left image shows overall thinning of retina (depicted by yellow and red codes in upper nomogram). Right image is for comparison showing normal thickness of retina depicted by normal green code in the nomogram.

Conclusion:

1-Retina as a part of eyes can medicate with one or a few session by OCT resourcefully.

2-we wrote about structure of eyes and diseases and about OCT device historically and physically and models by years also collected data of patient and compared with normal eyes.

3- optical coherence tomography is very amazing device we noticed and learned information and working also about laser ranges that going to use at OCT.

4- In next job I think that could research about different types by years and inside the device with working and the laser that used for it.

❖ Reference:

Rosenfeld, P.J., 2016. Optical coherence tomography and the development of antiangiogenic therapies in neovascular age-related macular degeneration. *Investigative ophthalmology & visual science*, *57*(9), pp.OCT14-OCT26.

Olson, J., Sharp, P., Goatman, K., Prescott, G., Scotland, G., Fleming, A., Philip, S., Santiago, C., Borooah, S., Broadbent, D. and Chong, V., 2013. Improving the economic value of photographic screening for optical coherence tomography-detectable macular oedema: a prospective, multicentre, UK study. *Health Technology Assessment*.

Kiernan, D.F., Mieler, W.F. and Hariprasad, S.M., 2010. Spectral-domain optical coherence tomography: a comparison of modern high-resolution retinal imaging systems. *American journal of ophthalmology*, *149*(1), pp.18-31.

Maloney, R., 2012. The Optovue iVue OCT System from Grafton Optical: the possibilities of hand-held OCT devices in ophthalmic practice. *Journal of Visual Communication in Medicine*, *35*(2), pp.76-81.

Liu, X., Kale, A.U., Capewell, N., Talbot, N., Ahmed, S., Keane, P.A., Mollan, S., Belli, A., Blanch, R.J., Veenith, T. and Denniston, A.K., 2019. Optical coherence tomography (OCT) in unconscious and systemically

unwell patients using a mobile OCT device: a pilot study. *BMJ open*, *9*(11), p.e030882.

Dayani, P.N., Maldonado, R., Farsiu, S. and Toth, C.A., 2009. Intraoperative use of handheld spectral domain optical coherence tomography imaging in macular surgery. *Retina*, *29*(10), pp.1457-1468.

Timoney, P.J. and Breathnach, C.S., 2013. Allvar Gullstrand and the slit lamp 1911. *Irish journal of medical science*, *182*, pp.301-305.

Walsh, A.C., 2011. Binocular optical coherence tomography. *Ophthalmic Surgery, Lasers and Imaging Retina*, *42*(4), pp.S95-S105.

Chopra, R., Mulholland, P.J., Dubis, A.M., Anderson, R.S. and Keane, P.A., 2017. Human factor and usability testing of a binocular optical coherence tomography system. *Translational Vision Science & Technology*, *6*(4), pp.16-16.

Chopra, R., Mulholland, P.J., Petzold, A., Ogunbowale, L., Gazzard, G., Bremner, F.D., Anderson, R.S. and Keane, P.A., 2020. Automated pupillometry using a prototype binocular optical coherence tomography system. *American Journal of Ophthalmology*, *214*, pp.21-31.

Chopra, R., Mulholland, P.J., Tailor, V.K., Anderson, R.S. and Keane, P.A., 2018. Use of a binocular optical coherence tomography system to evaluate strabismus in primary position. *JAMA ophthalmology*, *136*(7), pp.811-817.

Wittenborn, J.S., Clemons, T., Regillo, C., Rayess, N., Kruger, D.L. and Rein, D., 2017. Economic evaluation of a home-based age-related macular degeneration monitoring system. *Jama Ophthalmology*, *135*(5), pp.452-459.

Chew, E.Y., Clemons, T.E., Bressler, S.B., Elman, M.J., Danis, R.P., Domalpally, A., Heier, J.S., Kim, J.E., Garfinkel, R. and AREDS2-HOME Study Research Group, 2014. Randomized trial of a home monitoring system for early detection of choroidal neovascularization home monitoring of the Eye (HOME) study. *Ophthalmology*, *121*(2), pp.535-544.

Chopra, R., Wagner, S.K. and Keane, P.A., 2021. Optical coherence tomography in the 2020s—outside the eye clinic. *Eye*, *35*(1), pp.236-243.

Lally, D., Kim, J.E., Elman, M.J., Tomkins-Netzer, O., Alon, Y., Bergman, E. and Loewenstein, A., 2020. Performance of a novel deep learning algorithm for Automatic Retinal Fluid Quantification in Home OCT Images. *Investigative Ophthalmology & Visual Science*, *61*(7), pp.2571-2571.

Sudkamp, H., Koch, P., Spahr, H., Hillmann, D., Franke, G., Münst, M., Reinholz, F., Birngruber, R. and Hüttmann, G., 2016. In-vivo retinal imaging with off-axis full-field time-domain optical coherence tomography. *Optics Letters*, *41*(21), pp.4987-4990.

von der Burchard, C.C., Tode, J., Ehlken, C. and Roider, J., 2017. 2mm central macular volume scan is sufficient to detect exudative age-related macular degeneration activity in optical coherence tomography. *Investigative Ophthalmology & Visual Science*, *58*(8), pp.374-374.

Maloca, P., Hasler, P.W., Barthelmes, D., Arnold, P., Matthias, M., Scholl, H.P., Gerding, H., Garweg, J., Heeren, T., Balaskas, K. and de Carvalho, J.E.R., 2018. Safety and feasibility of a novel sparse optical coherence tomography device for patient-delivered retina home monitoring. Translational vision science & technology, 7(4), pp.8-8.

YOUNGQUIST, R.C., CARR, S. and Davies, D.E.N., 2001. Optical coherence-domain reflectometry: a new optical evaluation technique. *SPIE milestone series*, *165*, pp.119-121.

Gilgen, H.H., Novak, R.P., Salathe, R.P., Hodel, W. and Beaud, P., 2001. Submillimeter Optical Reflectometry. *SPIE milestone series*, *165*, pp.125-133.

Fercher, A.F., Mengedoht, K. and Werner, W., 2001. Eye-length measurement by interferometry with partially coherent light. *SPIE milestone series*, *165*, pp.246-248.

Huang, D., Wang, J., Lin, C.P., Puliafito, C.A. and Fujimoto, J.G., 1991. Micron-resolution ranging of cornea anterior chamber by optical reflectometry. *Lasers in surgery and medicine*, *11*(5), pp.419-425.

Bouma, B.E., Tearney, G.J., Bilinsky, I.P., Golubovic, B. and Fujimoto, J.G., 2001. Self phase-modulated Kerr-lens mode-locked Cr: forsterite laser source for optical coherence tomography. *SPIE milestone series*, *165*, pp.656-658.

Drexler, W., Morgner, U., Kärtner, F.X., Pitris, C., Boppart, S.A., Li, X.D., Ippen, E.P. and Fujimoto, J.G., 1999. In vivo ultrahigh-resolution optical coherence tomography. *Optics letters*, *24*(17), pp.1221-1223.